H_2O Condensation Coefficient and Refractive Index for Vapor-Deposited Ice from Molecular Beam and Optical Interference Measurements

D. E. Brown and S. M. George*

Department of Chemistry and Biochemistry, University of Colorado, Boulder, Colorado 80309-0215

C. Huang, E. K. L. Wong, Keith B. Rider, R. Scott Smith, and Bruce D. Kay*

Environmental Molecular Sciences Laboratory, Pacific Northwest National Laboratory, Richland, Washington 99352

Received: August 29, 1995; In Final Form: January 2, 1996[⊗]

The condensation of H_2O on ice multilayers on Ru(001) was studied using both molecular beam and optical interference techniques as a function of surface temperature. From the beam reflection technique, the H_2O sticking coefficient, S, was determined to be $S = 0.99 \pm 0.03$ at temperatures between 85 and 150 K and was independent of incident angle (0−70°) and beam energy (1−40 kcal/mol). The condensation coefficient, α, was dependent on both the incident H_2O flux and the desorption H_2O flux at the various surface temperatures. The magnitude of α varied continuously from unity at $T < 130$ K to zero at higher temperatures. The optical interference experiments yielded condensation coefficients and sticking coefficients of $\alpha = S = 0.97 \pm 0.10$ at temperatures from 97 to 145 K where the H_2O desorption flux was negligible with respect to the incident flux. The optical interference measurements monitored the ice film thickness versus H_2O exposure time and were dependent on the refractive index, n, and the density, ρ, of the vapor-deposited ice. Consequently, the combined molecular beam and optical interference measurements provided a means to evaluate the refractive index and density for vapor-deposited ice as a function of surface temperature. The values of the refractive index varied from $n = 1.27$ at 90 K to $n = 1.31$ at 130 K. The calculated densities varied from $\rho = 0.82$ g/cm^3 at 90 K to $\rho = 0.93$ g/cm^3 at 130 K. Previous optical interference data were also reanalyzed to yield refractive indices and ice densities for films grown at surface temperatures between 20 and 150 K. Both the refractive index and density increased monotonically with increasing growth temperature. The lower refractive index and density at lower temperatures indicate that microporous ice films are formed when H_2O deposits on substrates at $T < 120$ K.

I. Introduction

The condensation coefficient, α, of H_2O on ice has been the focus of numerous investigations.[1−23] The experimental values for the condensation coefficient have ranged from approximately $\alpha = 0.01$[2−4] to $\alpha = 1.0$.[5−7] Early investigations measured a variety of values for H_2O evaporation from both liquid and ice surfaces and assumed that the condensation coefficient was equivalent to the evaporation coefficient.[2−5,9−15] Direct measurements of the condensation coefficient[1,6−8,11,16−20] have not provided more consistent results and reported values have ranged from $\alpha = 0.026$[11] to $\alpha = 1.0$.[1,7,8]

Accurate measurement of the H_2O condensation coefficient on ice multilayers is very important to models of heterogeneous atmospheric chemistry. Reservoir chlorine species, such as chlorine nitrate ($ClONO_2$), are converted to active forms of chlorine, such as Cl_2, on polar stratospheric clouds (PSCs) composed of ice (type II) and H_2O/HNO_3 (type I) particles.[24−27] These active forms of chlorine can be photolyzed by sunlight and facilitate catalytic ozone destruction over the Antarctic. The H_2O condensation coefficient on ice is an important variable for PSC growth kinetics, and inaccuracies in α will effect the predictions from atmospheric models concerning PSC formation temperature, the size of PSC particles, and the lifetime of PSCs in the stratosphere.[28,29]

The condensation coefficient is defined as the ratio, $\alpha = C_{exp}/\Phi_{H_2O}$, between the experimentally observed growth rate, C_{exp}, and the maximum theoretical rate predicted by gas kinetic theory, Φ_{H_2O}. The maximum theoretical growth rate can be expressed as

$$\Phi_{H_2O} = \frac{P_v}{\sqrt{2\pi m k T_v}} \quad (1)$$

where P_v and T_v are the pressure and temperature of the impinging H_2O vapor, respectively. In the present study, molecular beam and optical interference techniques are both used to measure the H_2O condensation coefficient on ice multilayers grown on Ru(001). The molecular beam measurement of α relies on the beam reflection technique developed by King and Wells[30] to determine directly the H_2O condensation coefficient on ice. The optical interference technique obtains α by monitoring the reflectance of laser light from the ice−vacuum and the ice−substrate interfaces during the vapor deposition of ice multilayers.[1] The optical interference measurement is dependent on the refractive index and density of the vapor-deposited ice.

The molecular beam and optical interference techniques are independent measures of H_2O condensation. Because the molecular beam measurement of α is direct and therefore independent of the refractive index and density, this α can be used together with the optical interference data to determine the refractive index of vapor-deposited ice over the temperature range from 97 to 130 K. Subsequently, the Lorentz−Lorenz relationship can be employed to determine the corresponding ice density. These predicted refractive index and density values for vapor-deposited ice compare favorably with the few

[⊗] Abstract published in *Advance ACS Abstracts,* March 1, 1996.

0022-3654/96/20100-4988$12.00/0

experimentally measured values in this range. The temperature-dependent variation of the refractive index and density is significant, and earlier measurements that assumed constant refractive index and density are reevaluated in light of these new measurements.

II. Experimental Section

A. Molecular Beam Measurements. The experimental apparatus for the molecular beam measurements at Pacific Northwest National Laboratory has been described previously.[8] In brief, a quadruply differentially-pumped molecular beam of H_2O was used to dose the Ru(001) sample. For most of the experiments, the beam was quasi-effusive and had a velocity profile characteristic of a 300 K Maxwellian distribution. A variable energy (2−50 kcal/mol) supersonic nozzle beam source was also employed in several experiments. In all cases, the incident H_2O beam flux was between 10^{13} and 10^{14} molecules/(cm^2 s). The flux is defined in terms of ice monolayers where 1 ML = 1.056×10^{15} molecules/cm^2. This definition corresponds to the H_2O coverage in the $\sqrt{3} \times \sqrt{3}$ R30° ice-like bilayer on Ru(001)[31] with a Ru(001) lattice constant of a = 2.70 Å.[32]

This highly collimated beam has a circular profile of ∼0.35 cm diameter. This beam can intercept the ∼1.2 cm diameter Ru(001) sample at incident angles as large as 70° from the surface normal without overfilling the target. Dosing with this H_2O flux source enables precise and reproducible H_2O exposures to be attained without appreciable adsorption on surfaces other than the Ru(001) crystal. The beam dosing technique also allows the condensation coefficient to be determined directly by the beam reflection technique of King and Wells.[30] The incident, scattered, and desorbed fluxes of H_2O are detected in an angle-integrated manner by measuring the H_2O partial pressure in the scattering chamber with a quadrupole mass spectrometer. The mass spectrometer is positioned to prevent a line-of-sight view of the target surface and ensure that the detected signals are representative of the angle-integrated fluxes for all incident beam angles.

The Ru(001) single crystal resides in an UHV surface analytical chamber with a base pressure $<1 \times 10^{-10}$ Torr. The Ru(001) surface was cleaned and characterized by low-energy electron diffraction (LEED) and Auger electron spectroscopy (AES) using previously published procedures.[33] The crystal was attached to a liquid-nitrogen-cooled Dewar and was heated resistively. The sample temperature could be varied between 85 and 1500 K under computer control with a precision of better than ±0.1 K and an absolute accuracy of ±2 K.

B. Optical Interference Measurements. The optical interference experiments were performed in a second UHV chamber at the University of Colorado at Boulder that was pumped by a 200 L/s ion pump and titanium sublimation pumps that maintained a background pressure of at least $\leq 5 \times 10^{-9}$ Torr. The ice multilayers were deposited on a Ru(001) single-crystal substrate that was mounted on a liquid-nitrogen-cooled cryostat on a differentially pumped rotary feedthrough.[34] Analysis of surface cleanliness was monitored using AES with a single-pass cylindrical mirror analyzer and LEED spectrometry. The Ru(001) substrate was heated resistively and a W-5%Re/W-26%Re thermocouple was used to monitor surface temperature. The Ru(001) substrate was cleaned using standard cleaning procedures,[33] and AES confirmed that no carbon or oxygen remained on the surface following the cleaning procedure.

Distilled and deionized water was placed in a cold finger and additional purification was achieved by successive freeze−pump−thaw cycles to remove dissolved gases. Water vapor was then exposed to the Ru(001) crystal by backfilling the chamber to various pressures between $P = 1 \times 10^{-6}$ Torr and $P = 5 \times 10^{-5}$ Torr. The H_2O vapor pressures were measured using a Bayard-Alpert ion gauge. Ion gauge pressure readings are known to drift with time, and their absolute sensitivities can be in error by as much as ±50%.[35] Consequently, the ion gauge was calibrated using an absolute MKS Baratron with static water vapor pressures between 1×10^{-5} and 1×10^{-3} Torr. The calibration in this pressure regime was linear, and pressures below 1×10^{-5} Torr were determined by an extrapolation of the calibrated data.

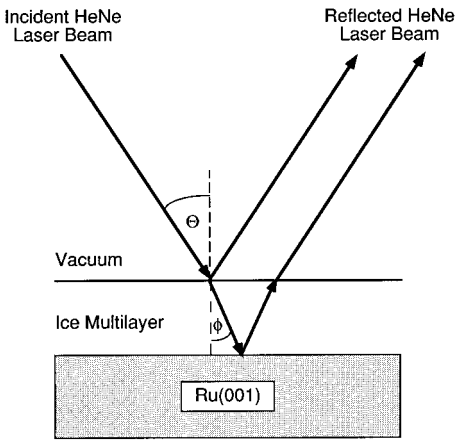

Figure 1. Geometry for the optical interference measurements of the growth of vapor-deposited ice multilayers on Ru(001). The reflections from the ice−vacuum and ice−Ru(001) interfaces versus multilayer thickness lead to constructive and destructive interference of the reflected He-Ne laser beam.

The optical interference technique has been described in detail previously.[1,36,37] Briefly, a Uniphase He-Ne laser with a wavelength of λ = 6328 Å was incident on the Ru(001) substrate at an incident angle of 2° from the surface normal. As a vapor-deposited ice multilayer grows, the beam is reflected at the ice−vacuum and ice−Ru(001) interfaces as shown in Figure 1. The interference between these reflections depends on the distance the beam travels through the ice multilayer and the refractive index of the ice film. As the H_2O vapor is deposited or removed via isothermal desorption, the intensity of the reflected He-Ne laser varies sinusoidally as the ice thickness changes linearly with time.

An EG&G FOD-100 photodiode detector was used to monitor the modulations in the He-Ne intensity versus ice multilayer thickness. The intensity of the He-Ne laser beam was attenuated with neutral density filters to prevent saturation of the photodiode. The optical interference signal from the photodiode was then digitized with a DSP Technology Model 1218 digitizer. To verify that the vapor-deposited ice films were growing uniformly across the Ru(001) substrate, the He-Ne laser beam diameter was varied from 1 to 10 mm, and no change was observed in the optical interference signal.

III. Results and Analysis

A. Molecular Beam Measurements. The condensation coefficient of H_2O on ice was measured using the molecular beam reflection technique.[30] A diagrammatic representation of the experiment is given in Figure 2. Impinging H_2O molecules can either reflect from the surface with flux J_{ref} or they can adsorb on the surface with flux J_{ads}. The sum of J_{ref} and J_{ads} is equal to the incident beam flux, J_{in}. The detected flux, J_{det}, is the sum of the angle-integrated fluxes of both the reflecting and desorbing H_2O molecules.

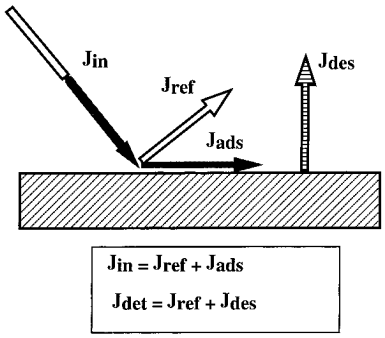

Figure 2. Representation of the H_2O fluxes in the molecular beam experiment. J_{in} and J_{ads} denote the H_2O flux incident and adsorbing on the ice surface, respectively. J_{ref} and J_{des} designate the H_2O flux reflected and desorbing from the ice surface, respectively.

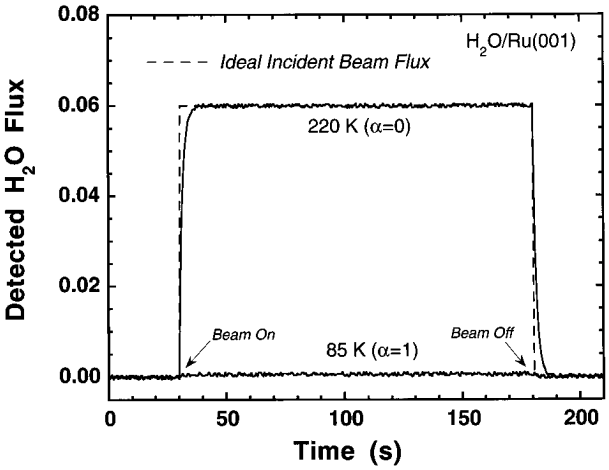

Figure 3. Molecular beam measurements of H_2O condensation on ice multilayers on Ru(001) at 85 and 220 K using the King and Wells reflection technique. The results are consistent with $\alpha = 1$ at 85 K and $\alpha = 0$ at 220 K.

The measurement of the H_2O condensation coefficient on ice for two substrate temperatures is displayed in Figure 3. The data at 220 K illustrate that the opening and closing of the H_2O beam produced an immediate rise and fall in H_2O signal intensity. The ideal waveform should be a square wave and is shown as a dashed line. At 220 K, the measured H_2O wave form has the same shape and intensity regardless of whether the sample Ru(001) target is in or out of the incident beam path. The small deviations between the measured wave form and the idealized square wave are due to the finite pump-out time and wall effects of the UHV chamber. These results at 220 K indicate that the detected H_2O flux is equal to the incident beam flux. Consequently, the condensation coefficient is $\alpha = 0$ at 220 K for an incident flux of 0.06 ML/s.

The data at 85 K show a very small detected H_2O flux signal that is <0.5% of the incident beam intensity upon opening the beam shutter. In this case, nearly all of the impinging H_2O molecules adsorb onto the surface, and the condensation coefficient is nearly unity. The small detected flux is probably an experimental artifact originating from a very weak uncollimated effusive beam issuing from the differential pumping chamber immediately upstream of the UHV scattering chamber. On the sole basis of this data at 85 K, the H_2O condensation coefficient is $\alpha \geq 0.995$.

The results at 85 K displayed in Figure 3 show that the condensation coefficient is independent of the amount of H_2O adsorbed. This behavior is revealed by the fact that the detected flux is constant in time despite the continuous adsorption of water on the Ru(001) substrate. This result allowed $\alpha(T)$ to be determined by measuring $J_{det}(T)$ according to eq 2 as the sample temperature was slowly ramped from high temperature (160 K) to low temperature (85 K):

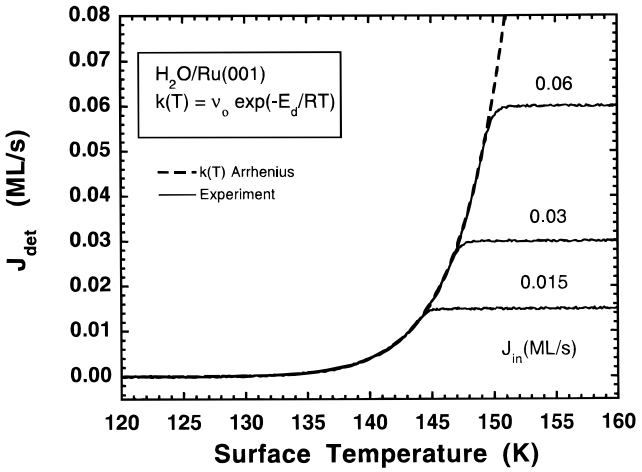

Figure 4. Temperature-dependent detected H_2O flux, $J_{det} = J_{ref} + J_{des}$, for incident H_2O beam fluxes of $J_{in} = 0.015$, 0.03, and 0.06 ML/s. The plateau regions at higher temperatures occur when $J_{det} = J_{in}$. As indicated by the dashed line, the three J_{det} curves can be described by zero-order desorption kinetics with a preexponential of $\nu_0 = (4.0 \pm 1.0) \times 10^{15}$ ML/s and a desorption activation barrier of $E_d = 48.25 \pm 0.80$ kJ/mol.

$$\alpha(J_{in},T) = \frac{J_{in} - J_{det}(T)}{J_{in}} = \frac{J_{ads}(T) - J_{des}(T)}{J_{in}} \qquad (2)$$

A slow cooling ramp of -0.02 K/s was used to ensure equilibrium throughout the entire measurement and to increase the signal-averaging time. A number of experiments verified that the measurements were independent of the cooling rate, incident beam energy (1−40 kcal/mol), and incident angle (0−70°).

Figure 4 displays the temperature-dependent detected flux, $J_{det}(T)$, for three different incident H_2O beam fluxes. All three curves show a plateau region at temperatures above 150 K but with the height of the plateau dependent on the incident H_2O beam flux. In this temperature region $J_{det}(T)$ is equal to J_{in}, indicating no net adsorption of H_2O on the surface. Upon further cooling $J_{det}(T)$ decreases to zero, indicating net adsorption of H_2O on the surface with the condensation coefficient, α, increasing from zero to unity.

As shown schematically in Figure 2, the experimentally measured $J_{det}(T)$ can have two contributions. The first contribution is from the reflected signal, J_{ref}, that is defined as $J_{ref} = J_{in} - J_{ads}$. The other contribution is from the desorption flux, J_{des}. Figure 4 reveals that the low-temperature, leading edge regions of the various curves are aligned at different incident beam fluxes. This alignment requires that the J_{ref} contribution be nearly zero for all temperatures below the plateau region observed at higher temperatures. The requirement that $J_{ref} \approx 0$ is necessary because the magnitude of J_{ref} is directly proportional to J_{in}. If J_{ref} were nonzero, the absolute magnitude of J_{ref} would be different for the three J_{in} curves and lead to a lack of alignment in the leading edge region of Figure 4. $J_{ref} \approx 0$ implies that the adsorption probability is near unity and independent of both temperature and flux.

Because $J_{det}(T)$ is independent of the incident H_2O flux in the leading edge region, the observed temperature dependence must be attributed only to the desorption flux. The leading edge region of Figure 4 readily lends itself to an Arrhenius kinetic analysis where the H_2O desorption flux follows zero-order

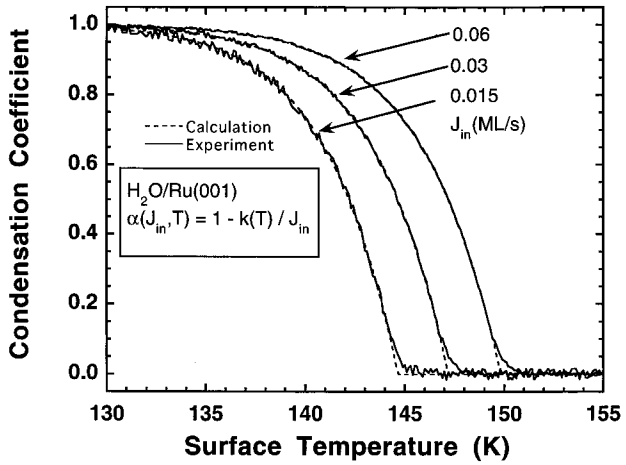

Figure 5. Temperature-dependent condensation coefficient for H_2O on ice multilayers grown on Ru(001) determined by the molecular beam experiments using eq 2.

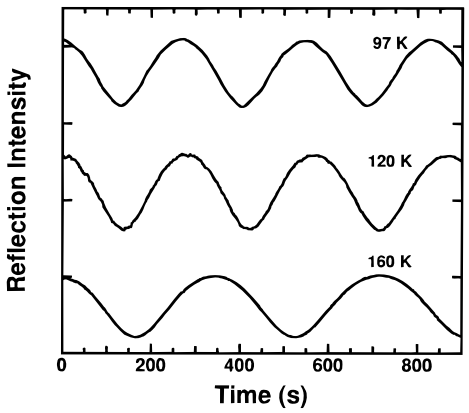

Figure 6. Reflection intensity of the He-Ne laser beam versus time during H_2O condensation on ice multilayers on Ru(001) at $P_{H_2O} = 5.5 \times 10^{-6}$ Torr and surface temperatures of 97, 120, and 160 K. The reflectance oscillates as a result of constructive and destructive optical interference during the ice multilayer growth.

kinetics, $-d\Theta/dt = \nu_0 \exp[-E_d/RT]$. The dashed line displayed in Figure 4 shows clearly that all the J_{in} curves are described by a single set of Arrhenius parameters with $\nu_0 = (4.0 \pm 1.0) \times 10^{15}$ ML/s and $E_d = 48.25 \pm 0.80$ kJ/mol. These kinetic parameters are in excellent agreement with previous measurements of H_2O desorption from ice multilayers.[1]

The temperature-dependent condensation coefficient, $\alpha(J_{in},T)$, can be calculated from the experimental data using eq 2. The results of these calculations are displayed graphically in Figure 5. For all J_{in} fluxes, the condensation coefficient is $\alpha \approx 1$ below 130 K. The condensation coefficient decreases monotonically and smoothly to zero at higher temperatures, and the temperature at which $\alpha \approx 0$ increases with increasing incident beam flux. The observed temperature dependence of the condensation coefficient, $\alpha(J_{in},T)$, can be readily understood by examining eq 2.

Equation 2 indicates that $\alpha(J_{in},T)$ is simply related to the adsorption and desorption H_2O fluxes. For the case when $J_{ads} = J_{des}$, the condensation coefficient is zero. Note that a condensation coefficient of zero does not necessarily imply that molecules from the incident beam are not temporarily trapping, but only that $J_{ads} = J_{des}$. When no desorption takes place, $J_{des} = 0$, and the condensation coefficient is equal to the conventional definition of the sticking coefficient, $S = J_{ads}/J_{in}$ and is independent of incident beam flux. Substitution of $S(T) = J_{ads}(T)/J_{in}$ into eq 2 yields

$$\alpha(J_{in},T) = S(T) - \frac{J_{des}(T)}{J_{in}} \tag{3}$$

At temperatures <130 K, the desorption flux is small with respect to the incident flux ($J_{des} \ll J_{in}$), and both the sticking and condensation coefficients are near unity and temperature independent. As $J_{des}(T)$ increases, the condensation coefficient $\alpha(J_{in},T)$ decreases until $J_{des} = J_{in}$, at which point $\alpha(J_{in},T) = 0$. Since J_{des} depends only on temperature, the condensation coefficient exhibits a flux dependence. At all temperatures where the condensation coefficient is nonzero, the experimental data displayed in Figure 4 require that $S(T) \approx 1$. A calculation of $\alpha(J_{in},T)$ using eq 3 with $S(T) = 1$ and J_{des} calculated from the Arrhenius parameters is shown in Figure 5 by the dashed lines. The calculated and experimental curves are in excellent agreement.

B. Optical Interference Measurements. Figure 6 shows representative optical interference signals versus time during H_2O condensation on ice multilayers at surface temperatures of 97, 120, and 160 K. The interference signal intensity modulates as a result of constructive and destructive interference.[1,37] This interference modulates the reflectance of the He-Ne laser beam from the ice−vacuum and the ice−Ru(001) interfaces by ~20%. The sinusoidal nature of the interference signal indicates a constant growth rate of the ice multilayer on Ru(001) that is independent of ice multilayer thickness.[1]

Additional reflectance measurements were obtained for temperatures from 97 to 180 K at temperature increments of approximately 5 K. The H_2O vapor pressure was 5.5×10^{-6} Torr for the optical interference experiments performed between 97 and 160 K. The slower oscillation frequency of the interference signal observed in Figure 6 for H_2O condensation at 160 K is indicative of slower ice multilayer growth caused by simultaneous H_2O desorption occurring at this higher temperature. To overcome increased H_2O desorption rates at higher temperatures, the H_2O vapor pressure was increased for the interference experiments above 160 K. The H_2O vapor pressure was $P = 1.1 \times 10^{-5}$ Torr at 165 K, 1.5×10^{-5} Torr at 170 K, 1.8×10^{-5} Torr at 175 K, and 4.6×10^{-5} Torr at 180 K.

The rate of H_2O condensation was obtained from the frequency of modulation of the optical interference signal versus time. Constructive interference of the He-Ne laser beam reflected from both the ice−vacuum and ice−Ru(001) interfaces occurs when the path length traveled through the ice multilayer is an integral number of wavelengths. The ice multilayer thickness corresponding to adjacent maxima in the optical interference signal can be calculated using[1]

$$x = \frac{\lambda}{2n(T)\cos\phi} \tag{4}$$

where x is the ice thickness in Å, $\lambda = 6328$ Å is the wavelength of the He-Ne, laser, $n(T)$ is the temperature-dependent refractive index of the ice film, and φ is the angle of incidence relative to the Ru(001) surface as shown in Figure 1.

The vapor-deposited ice multilayer structure that grows during H_2O condensation is dependent on surface temperature. Microporous ice with surface areas on the order of 400 m^2/g and pore widths less than 2 nm has been observed at temperatures ≤90 K.[38] This porous structure is consistent with the reported refractive indices of $n(77\text{ K}) = 1.275$[39] and $n(90\text{ K}) = 1.27$ for microporous ice.[37] In contrast, the ice film is crystalline at 160 K and has a refractive index of $n(160\text{ K}) = 1.31$. The transition

from microporous to crystalline ice has not been carefully characterized as a function of surface temperature. The refractive index of ice grown at 130 K has been measured to be $n(130\ \mathrm{K}) = 1.31$ using optical interference.[37] Although these ice films at 130 K were probably not completely crystalline, they have a refractive index that is nearly equal to the refractive index of crystalline ice. This index is consistent with the collapse of the microporous ice upon annealing that produces a dense ice film.[38]

The analysis of the optical interference data assumed a linear interpolation between the measured values of the refractive index of ice at 90 and 130 K. Above 130 K, the value of the refractive index for ice was assumed to remain constant at $n(\geq 130\ \mathrm{K}) = 1.31$. The angle of incidence of the He-Ne laser on the Ru(001) substrate after passing through the ice film can be determined using Snell's Law, $\sin\Theta = n(T)\sin\varphi$, where Θ is the angle of incidence of the He-Ne laser relative to the ice multilayer. Using $\Theta = 2.0°$ and the temperature-dependent refractive index, $n(T)$, the angle of incidence relative to the Ru(001) surface ranged between $\varphi = 1.5°$ at 97 K and $\varphi = 1.6°$ at $T \geq 130$ K. The ice multilayer thickness corresponding to adjacent maxima in the optical interference signal also varied from $x = 2492$ Å at 83 K to $x = 2416$ Å at $T \geq 130$ K because of the temperature-dependent refractive index.

The rate of H_2O condensation can be expressed as

$$\frac{\mathrm{d}x}{\mathrm{d}t} = \left(\frac{\alpha}{\rho(T)}\right)\Phi_{H_2O} \tag{5}$$

where $\mathrm{d}x/\mathrm{d}t$ is the experimentally observed H_2O condensation rate in cm/s and $\rho(T)$ is the temperature-dependent ice density. Although the density of crystalline ice is known, very few experiments have studied the temperature-dependent density of vapor-deposited ice as a function of surface temperature.[36,40] In particular, there are almost no density measurements for amorphous or microporous ices formed at low surface temperatures.

The Lorentz−Lorenz equation can be used to determine $\rho(T)$ from $n(T)$:[41,42]

$$R = \left(\frac{1}{\rho(T)}\right)\left(\frac{n(T)^2 - 1}{n(T)^2 + 2}\right) \tag{6}$$

The specific refraction, R, can be determined from eq 6 using known values of the density and refractive index at a single temperature. At 160 K, the refractive index of crystalline ice is $n(160\ \mathrm{K}) = 1.31$[37] and is equivalent to the refractive index of crystalline ice.[43,44] Consequently, the density of vapor-deposited ice at 160 K is assumed to be $\rho(160\ \mathrm{K}) = 0.93\ \mathrm{g/cm^3}$. The resulting value of the specific refraction is $R = 0.2072\ \mathrm{cm^3/g}$. This specific refraction is in excellent agreement with previously measured values[44] and verifies the assumption that $\rho(160\ \mathrm{K}) = 0.93\ \mathrm{g/cm^3}$. Using this value of the specific refraction, $\rho(T)$ was determined from eq 6 using the interpolated values of the temperature-dependent refractive index, $n(T)$.

The condensation coefficient can then be determined from eq 5 using $\rho(T)$ and the measured $\mathrm{d}x/\mathrm{d}t$ values from the optical interference measurements. The H_2O condensation coefficients versus surface temperature from 100 to 160 K are shown in Figure 7. The average value of the condensation coefficient from 97 to 145 K is $\alpha = 0.97 \pm 0.10$. Because the H_2O desorption flux is negligible for $T < 130$ K, the condensation coefficient equals the sticking coefficient and $\alpha = S = 0.97 \pm 0.10$. Above 130 K, the condensation coefficient is dependent on the magnitude of the incident H_2O flux. The measured values shown in Figure 7 are for an incident H_2O flux of 2.6×10^{15} molecules/(cm^2 s) corresponding to a H_2O absolute pressure of 5.5×10^{-6} Torr at 300 K. The solid line represents the condensation coefficient predicted by eq 3 using $S = 0.97$, $J_{des}(T)$ determined by the zero-order desorption kinetics and an H_2O gas temperature of 300 K. The condensation coefficients measured at 160 K $< T <$ 180 K and higher H_2O vapor pressures were consistent with eq 3 using $S = 1$ and J_{des} determined by the zero-order desorption parameters.

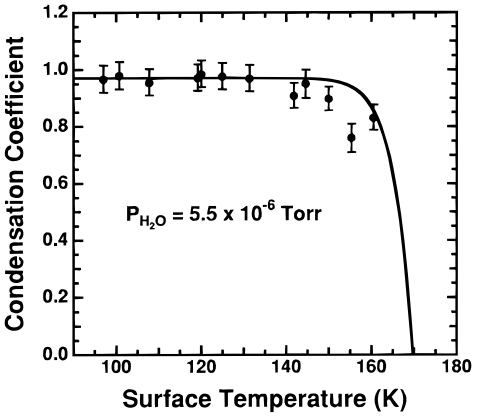

Figure 7. Condensation coefficient for H_2O on ice multilayers on Ru(001) measured at $P_{H_2O} = 5.5 \times 10^{-6}$ Torr using the optical interference technique. The solid line represents the condensation coefficient predicted by eq 3 using $S = 0.97$, $J_{des}(T)$ determined by the zero-order desorption kinetics, and an H_2O gas temperature of 300 K.

IV. Discussion

A. H_2O Condensation Coefficient on Vapor-Deposited Ice. An important distinction should be made between the sticking coefficient, S, and the condensation coefficient, α. The sticking coefficient is defined as $S = J_{ads}/J_{in}$ and is a measure of the adsorption probability. The condensation coefficient is defined by eq 2 and is a measure of the net adsorption flux ($J_{ads} - J_{des}$). The relationship between S and α is given by eq 3. Equation 3 indicates that S will always be greater than or equal to α. The results show that the sticking coefficient for H_2O on vapor-deposited ice is $S \approx 1$ and is temperature-independent.

In contrast to the sticking coefficient, the condensation coefficient varies from unity to zero depending on the surface temperature and H_2O flux. When the desorption flux is much smaller than the incident flux, S and α are nearly equal. At temperatures where the desorption flux approaches the incident flux, the condensation coefficient will approach zero. A condensation coefficient of zero does not mean that the sticking coefficient is zero, but only that there is no net change in the film thickness.

The H_2O condensation coefficient on ice can be calculated over a wide range of incident H_2O fluxes, J_{in}, using eq 3. Equation 3 can be expressed in terms of H_2O partial pressure by substitution of eq 1 for J_{in}. Figure 8 displays the H_2O condensation coefficient as a function of temperature for H_2O partial pressures between $P_{H_2O} = 1 \times 10^{-10}$ and 10 Torr. These calculations were performed assuming a temperature-independent $S = 1$ and zero-order desorption kinetic parameters for H_2O desorption from ice of $\nu_0 = (4.0 \pm 1.0) \times 10^{15}$ ML/s and $E_d = 48.25 \pm 0.80$ kJ/mol. Figure 8 shows that the threshold where the condensation coefficient varies from unity to zero is shifted to higher temperatures at higher H_2O pressures (fluxes). The vapor pressure of ice can also be calculated from the H_2O desorption kinetics assuming $S = 1$. The calculated vapor pressure is found to be in excellent agreement with measured

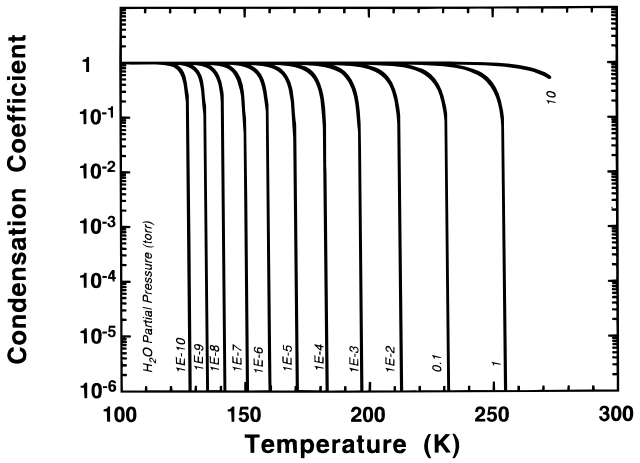

Figure 8. Condensation coefficient for H_2O on ice multilayers versus temperature calculated using eq 3 for H_2O vapor pressures between 1 $\times$ 10^{-10} and 10 Torr. This calculation assumes equivalent gas and surface temperatures, $S = 1$ and $J_{des}(T)$ described by the zero-order desorption kinetics, $\nu_0 = (4.0 \pm 1.0) \times 10^{15}$ ML/s, and $E_d = 48.25 \pm 0.80$ kJ/mol.

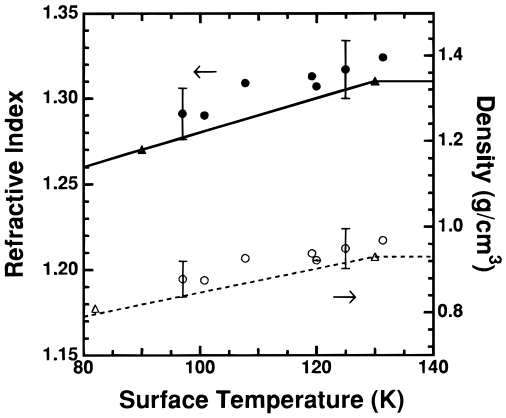

Figure 9. Refractive index (solid circles) and density (open circles) of vapor-deposited ice versus surface temperature determined by the combined molecular beam and optical interference measurements. The solid and dashed lines represent the temperature-dependent refractive index and density, respectively, that were utilized in the optical interference analysis. The triangles are previous literature values of these quantities.

values up to the melting point (273 K) and indicates that the sticking coefficient is near unity and temperature-independent over the range 80−273 K.[45]

Both the molecular beam and optical interference techniques measured a H_2O condensation coefficient of $\alpha \approx 1$ on ice at $T < 130$ K as shown in Figures 5 and 7. Above 130 K, the value of the condensation coefficient was reduced because of competing H_2O desorption. Several previous investigations of H_2O condensation on both liquid and ice surfaces have measured high condensation coeffients of $\alpha \geq 0.5$.[1,5,6,20,21] However, numerous other studies have measured $\alpha < 0.5$ and values as low as $\alpha = 0.01$.[1] As clearly shown by eq 3 and Figure 8, these discrepancies can possibly be understood by realizing that the condensation coefficient is both a function of surface temperature and incident H_2O flux.

A high H_2O sticking coefficient on ice multilayers would be expected from a soft cube model of energy accommodation for a molecule impinging on a surface.[46] A vapor phase H_2O molecule approaching the ice surface with a thermal energy of ~300 K would be greatly accelerated toward the ice surface by the ~12 kcal/mol attractive potential well.[1,47] Maximum energy transfer is expected for a molecule that collides with a surface composed of molecules with an equivalent mass.[46,48] The efficient energy transfer between the impinging H_2O molecule and the surface is then sufficient to prevent escape from the attractive potential well.

The bond between the incident H_2O molecule and the ice surface will initially contain the excess kinetic energy of ~12 kcal/mol resulting from the new hydrogen bonds. Simulations have shown that this excess energy is converted to highly excited adsorbate−surface vibrational modes.[47] These excited vibrational modes are strongly coupled to a continuum of bulk states in the underlying ice multilayer that are composed of similar modes.[49,50] This energy relaxation should be very rapid and lead to facile energy transfer. Efficient energy transfer to the liquid H_2O surface has also been observed in measurements of the interfacial heat transfer resistance of H_2O vapor condensing on liquid H_2O surfaces.[15,51]

B. Real Refractive Index and Density of Ice. The molecular beam and optical interference techniques provide two independent measurements of the condensation coefficient. The condensation coefficient measured by the optical interference method is dependent upon $n(T)$ and $\rho(T)$. Consequently, the absolute α determined by the molecular beam experiments can be used to solve for $n(T)$ and $\rho(T)$ in the equations describing the optical interference.

The change in ice multilayer thickness versus time is described by eq 5 where $\Phi_{H_2O} = 2.6 \times 10^{15}$ molecules/(cm^2 s) for the optical interference measurements. dx/dt can also be expressed as the ice thickness, Δx, grown during one complete interference cycle in the time period, Δt. Substituting for Δx in eq 5 using eq 4 allows eq 5 to be rewritten as

$$\left(\frac{\lambda}{2n(T)\cos\phi}\right) = \left(\frac{\alpha}{\rho(T)}\right)\Phi_{H_2O}\,\Delta t \qquad (7)$$

The only two variables in this expression that are not directly measured are $n(T)$ and $\rho(T)$. The condensation coefficient, $\alpha \approx 1$, is obtained from the molecular beam experiments and eq 3 using the appropriate incident H_2O flux. The angle ϕ is close to the surface normal, and $\cos\phi \approx 1$.

The density, $\rho(T)$, can be expressed in terms of the refractive index, $n(T)$, using eq 6 for the specific refraction, R. Consequently, eq 7 can be reduced to an equation with a single unknown, $n(T)$:

$$\left(\frac{\lambda}{2n(T)\cos\phi}\right) = \alpha R\left(\frac{n(T)^2+2}{n(T)^2-1}\right)\Phi_{H_2O}\,\Delta t \qquad (8)$$

For $\alpha \approx 1$ and $\lambda/(2n(T)\cos\phi)$ and Δt from the optical interference experiments, eq 8 can be solved for $n(T)$ because all the other terms are constant.

The calculated temperature-dependent refractive indices, $n(T)$, at $\lambda = 6328$ Å for the vapor-deposited ice multilayers grown between 97 and 130 K are shown in Figure 9. The error bars represent approximately ±4% error in Φ_{H_2O} based on the absolute uncertainties of the MKS Baratron that was used to calibrate the ionization gauge. The solid circles are the calculated values from the optical interference data, and the solid triangles represent the previous literature data.[37] The refractive indices used in the determination of the condensation coefficient from the optical interference experiments are shown as the solid line.

The values of the temperature-dependent density, $\rho(T)$, of the vapor-deposited ice multilayers can subsequently be determined from the corresponding refractive indices using the Lorentz−Lorenz equation given by eq 6. These densities are shown as

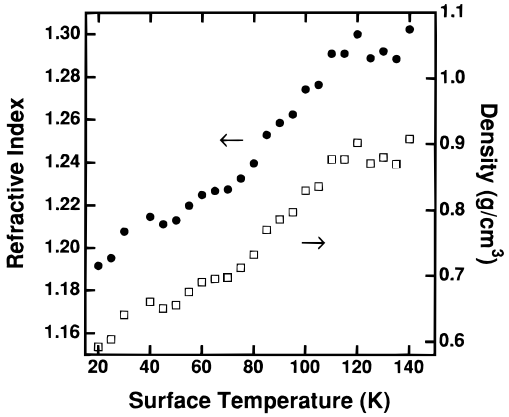

Figure 10. Reevaluation of previous optical interference measurements (ref 1) to determine the refractive index (solid circles) and density (open squares) of vapor-deposited ice versus surface temperature. This reinterpretation assumed $S = \alpha = 1$ and a refractive index of $n = 1.27$ and a density of $\rho = 0.82$ g/cm^3 at 90 K.

the open circles in Figure 9. The error bars again represent the ±4% error in Φ_{H_2O} based on the uncertainties of the MKS Baratron. The open triangles are the previous literature data.[36,37] The dashed line represents the densities used to calculate the condensation coefficient from the optical interference measurements.

The calculated values of the refractive index and density for vapor-deposited ice using the combined molecular beam and optical interference measurements are in good agreement with the few previous measurements. The calculated refractive indices and densities are slightly higher than the values based on interpolation from earlier literature values. These higher values can be explained if the H_2O flux measured by the calibrated ionization gauge was systematically high by ~3%. The values for the temperature-dependent refractive index and density shown in Figure 9 are also in good correspondence with recent measurements of the refractive index of vapor-deposited ice at $\lambda = 6328$ Å using the optical interference technique and Fresnels' equations.[52] The temperature-dependence of the refractive index of ice in the infrared has also been obtained recently from aerosol extinction spectra.[53]

C. Reinterpretation of Previous Results. A condensation coefficient of $\alpha \approx 1$ is in conflict with previous measurements over the same temperature range using the optical interference technique.[1] This disagreement can be understood by examining the assumptions made in the earlier optical interference analysis. Values of the refractive index and density for ice were assumed to be constant at $n = 1.31$ and $\rho = 0.93$ g/cm^3 over the entire temperature range.[1] These previous assumptions are not justified given the results in this paper and recent refractive index measurements.[52] One artifact of these assumptions was a slight temperature dependence of the condensation coefficient that was interpreted using a precursor-mediated adsorption model.[1]

The earlier condensation coefficients can be reanalyzed assuming a condensation coefficient $\alpha = 1$, a refractive index $n = 1.27$, and a density $\rho = 0.82$ g/cm^3, at 90 K.[37] These assumptions allow the flux, Φ_{H_2O}, that is consistent with $\alpha = 1$ to be calculated directly. Subsequently, this corrected flux can be utilized together with the earlier optical interference measurements and $\alpha = 1$ to calculate the temperature dependence of the refractive index and density of vapor-deposited ice. The refractive index and density for temperatures from 20 to 160 K are shown in Figure 10. There is very good agreement between the reanalysis of these earlier measurements displayed in Figure 10 and the results of the current study shown in Figure 9.

Figure 10 reveals that the refractive index and density of ice decrease continuously at progressively lower surface temperatures. The lower densities indicate that the ice films have extremely high porosities. A density of $\rho = 0.6$ g/cm^3 at 20 K is consistent with a porosity of 35% compared with crystalline ice at 160 K. In agreement with the recent refractive index measurements,[52] these results demonstrate that ice formed when H_2O deposits on substrates at $T < 120$ K is microporous and will inevitably have surface areas that are much greater than a single-crystal surface.

V. Conclusions

The condensation of H_2O on ice multilayers deposited on Ru(001) has been examined using molecular beam and optical interference techniques. The sticking coefficient for H_2O on vapor-deposited ice is unity and independent of incident beam flux, beam energy (1−40 kcal/mol), and surface temperature. The condensation coefficient was found to be dependent on the incident beam flux and surface temperature. Equation 3 can be used to calculate the H_2O condensation coefficient given the incident flux and surface temperature. This equation can easily be converted to H_2O partial pressure (see Figure 8) and may be useful in modeling the polar stratospheric clouds (PSCs) that are implicated in the Antarctic ozone hole.

The values for $\alpha(T)$ determined by the optical interference technique depend on the temperature-dependence of the refractive index, $n(T)$, and density, $\rho(T)$, of vapor-deposited ice. The condensation coefficient determined by the molecular beam experiments and represented by eq 3 was used to solve for $n(T)$ and $\rho(T)$ using the optical interference measurements. This determination utilized the Lorentz−Lorenz equation for the relationship between the refractive index and density. The temperature-dependent refractive index and density for vapor-deposited ice were determined in the temperature regime from 97 to 130 K where ice becomes increasingly porous at lower temperatures. These calculated values were in good agreement with the few existing literature measurements.

Previous investigations of the H_2O condensation coefficient on ice multilayers at 20 K < T < 185 K using optical interference techniques were also reevaluated assuming that $S = 1$. These earlier measurements also yielded temperature-dependent refractive indices and densities in good agreement with the current study. The refractive index varied from $n = 1.19$ at 20 K to $n = 1.31$ at 140 K. The density varied from $\rho = 0.6$ g/cm^3 at 20 K to $\rho = 0.9$ g/cm^3 at 140 K. These values indicate that vapor-deposited ice becomes increasingly porous for H_2O adsorption at lower substrate temperatures and a high porosity of ~35% is obtained at 20 K.

Acknowledgment. The optical interference portion of this work was performed at the University of Colorado and was supported by the National Science Foundation under Grant No. CHE-9215247. S.M.G. thanks the National Science Foundation for a Presidential Young Investigator Award (1988−1994). D.E.B. thanks the National Science Foundation for an Atmospheric Training Grant (1994−1995). The molecular beam portion of this work was performed at Pacific Northwest National Laboratory and was supported by the Chemical Physics Program of the Chemical Sciences Division of the Department of Energy Office of Basic Energy Science. Pacific Northwest National Laboratory is operated for the U.S. Department of Energy by Battelle under contract DE-AC06-76RLO 1830. One

of us (K.B.R.) gratefully acknowledges support from the Department of Energy, Division of University and Industry Programs, Office of Energy Research, as a Science and Engineering Research Semester program participant at Pacific Northwest National Laboratory.

References and Notes

(1) Haynes, D. R.; Tro, N. J.; George, S. M. *J. Phys. Chem.* **1992**, *96*, 8502.
(2) Alty, T. *Proc. R. Soc. London A* **1931**, *131*, 554.
(3) Alty, T. *Philos. Mag.* **1933**, *15*, 82.
(4) Alty, T.; Mackay, C. A. *Proc. R. Soc. London* **1935**, *149*, 104.
(5) Levine, N. E. *J. Geophys. Res.* **1973**, *78*, 6266.
(6) Schulze, F.-W.; Cammenga, H. K. *Ber. Bunsen-Ges. Phys. Chem.* **1980**, *84*, 163.
(7) Tolbert, M. A.; Middlebrook, A. M. *J. Geophys. Res.* **1990**, *95*, 22423.
(8) Kay, B. D.; Lykke, K. R.; Creighton, J. R.; Ward, S. J. *J. Chem. Phys.* **1989**, *91*, 5120.
(9) Kramers, H.; Stemerding, S. *Appl. Sci. Res. A* **1953**, *3*, 73.
(10) Nabavian, K.; Bromley, L. A. *Chem. Eng. Sci.* **1963**, *18*, 651.
(11) Sinarwalla, A. M.; Alofs, D. J.; Carstens, D. J. *J. Atmos. Sci.* **1975**, *32*, 592.
(12) Narusawa, M.; Springer, G. S. *J. Colloid Interface Sci.* **1975**, *50*, 392.
(13) Delaney, L. J.; Houston, R. W.; Eagleton, L. C. *Chem. Eng. Sci.* **1964**, *19*, 105.
(14) Tamir, A.; Hasson, D. *Chem. Eng. J.* **1970**, *2*, 200.
(15) Mills, A. F.; Seban, R. A. *Int. J. Heat Mass Transfer* **1967**, *10*, 1815.
(16) Bonacci, J. C.; Myers, A. L.; Nongbri, G.; Eagleton, L. C. *Chem. Eng. Sci.* **1976**, *31*, 609.
(17) Chodes, N.; Warner, J.; Gagin, A. *J. Atmos. Sci.* **1974**, *31*, 1351.
(18) Leu, M.-T. *Geophys. Res. Lett.* **1988**, *15*, 17.
(19) Isono, K.; Iwai, K. *Nature* **1969**, *233*, 1149.
(20) Bryson, C. E., III; Cazcarra, V.; Levenson, L. L. *J. Vac. Sci. Technol.* **1974**, *11*, 411.
(21) Koros, R. M.; Deckers, J. M.; Andres, R. P.; Boudart, M. *Chem. Eng. Sci.* **1966**, *21*, 941.
(22) Hirth, J. P.; Pound, G. M. *Condensation and Evaporation*; Pergamon: Oxford, 1963.
(23) Pound, G. M. *J. Phys. Chem. Ref. Data* **1972**, *1*, 135.
(24) Tabazadeh, A.; Turco, R. P. *J. Geophys. Res.* **1993**, *98*, 12.
(25) Turco, R. P.; Toon, O. B.; Hamill, P. *J. Geophys. Res.* **1989**, *94*, 16493.
(26) Hanson, D. R.; Ravishankara, A. R. *J. Geophys. Res.* **1991**, *96*, 5081.
(27) Hanson, D. R.; Ravishankara, A. R. *J. Phys. Chem.* **1992**, *96*, 2682.
(28) Pruppacher, H. R.; Klett, J. D. *Microphysics of Clouds and Precipitation*; D. Reidel Publishing Co.: Dordrecht, Holland, 1980.
(29) Toon, O. B.; Turco, R. P.; Jordan, J.; Goodman, J.; Ferry, G. *J. Geophys. Res.* **1989**, *94*, 11359.
(30) King, D. A.; Wells, M. G. *Surf. Sci.* **1972**, *29*, 454.
(31) Doering, D. L.; Madey, T. E. *Surf. Sci.* **1982**, *123*, 305.
(32) Grant, J. T.; Haas, T. W. *Surf. Sci.* **1970**, *21*, 76.
(33) Deckert, A. A.; Brand, J. L.; Arena, M. V.; George, S. M. *Surf. Sci.* **1989**, *208*, 441.
(34) George, S. M. *J. Vac. Sci. Technol. A* **1986**, *4*, 2394.
(35) Winkler, A.; Rendulic, K. D.; Wendl, K. *Appl. Surf. Sci.* **1982**−**3**, *14*, 209.
(36) Seiber, B. A.; Wood, B. E.; Smith, A. M. *Science* **1970**, *170*, 652.
(37) Berland, B. S.; Haynes, D. R.; Foster, K. L.; Tolbert, M. A.; George, S. M.; Toon, O. B. *J. Phys. Chem.* **1994**, *98*, 4358.
(38) Rowland, B.; Devlin, J. P. *J. Chem. Phys.* **1991**, *94*, 812.
(39) Browell, E. V.; Anderson, R. C. *J. Opt. Soc. Am.* **1975**, *65*, 919.
(40) Bar-Nun, A.; Dror, J.; Kochavi, E.; Laufer, D. *Phys. Rev. B* **1987**, *35*, 2427.
(41) Bottcher, C. J. F. *Theory of Electric Polarization*; Elsevier Publishing: Amsterdam, 1952.
(42) Born, M.; Wolf, E. *Principles of Optics*; Pergamon Press: Oxford, 1975.
(43) Warren, S. G. *Appl. Opt.* **1984**, *23*, 1206.
(44) Eisenberg, D.; Kauzmann, W. *The Structure and Properties of Water*; Oxford University Press: New York, 1969.
(45) *CRC Handbook of Chemistry and Physics*; CRC Press, Inc.: Boca Raton, FL, 1983−4).
(46) Steinbrüchel, C.; Schmidt, L. D. *J. Phys. Chem. Solids* **1973**, *34*, 1379.
(47) Tully, J. C. *Faraday Discuss. Chem. Soc.* **1985**, *80*, 291.
(48) Barker, J. A.; Auerbach, D. J. *Surf. Sci. Rep.* **1985**, *4*, 1.
(49) Brivio, G. P.; Grimley, T. B. *Surf. Sci. Rep.* **1993**, *17*, 1.
(50) Kreuzer, H. J.; Gortel, Z. W. In *Physisorption Kinetics*; Springer-Verlag: Berlin, 1986.
(51) Wenzel, H. *Int. J. Heat Mass Trans.* **1969**, *12*, 125.
(52) Berland, B. S.; Brown, D. E.; Tolbert, M. A.; George, S. M. *Geophys. Res. Lett.* **1995**, *22*, 3493.
(53) Clapp, M. L.; Miller, R. E.; Worsnop, D. R. *J. Phys. Chem.* **1995**, *99*, 6317.

JP952547J